Efficient electroreduction of carbonyl compounds to alcohols over Fe/Fe$_2$O$_3$ interfaces

Jin Lin[1,4], Zhenpeng Liu[1,4], Haofei Wu[2], Zhiqi Wang[1], Guangqiu Wang[1], Ju Bu[1], Yanan Wang[3], Pan Liu[2] ✉, Junjie Wang[2] & Jian Zhang[1] ✉
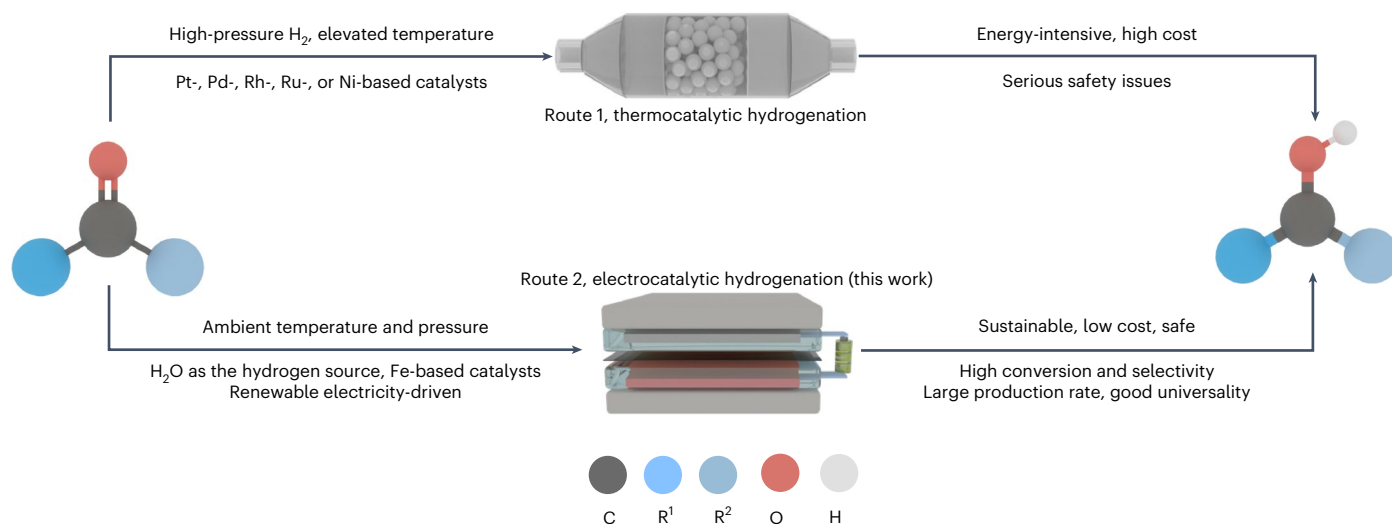
Catalytic hydrogenation of carbonyl compounds is widely used in chemical manufacturing and biomass refining, but current thermocatalytic processes require elevated temperatures, high-pressure H$_2$ and expensive catalysts. Here we demonstrate an electroreduction of carbonyl compounds over Fe/Fe$_2$O$_3$ interfaces in Fe/Fe$_2$O$_3$ nanoarrays (Fe/Fe$_2$O$_3$ NAs), where Fe and Fe$_2$O$_3$ species synergistically accelerate the kinetics of acetone hydrogenation by promoting acetone adsorption and H* formation. With acetone as the probe molecule, an isopropanol partial current density of 1.6 A cm^{-2} and ~100% selectivity are achieved in 1 M KOH aqueous solution. Even in a large-scale, two-electrode electrolyser, Fe/Fe$_2$O$_3$ NAs stably deliver an acetone conversion of >99%, an isopropanol selectivity of 100%, and an isopropanol production rate of 21.6 g g$_{cat}^{-1}$ h^{-1} at 0.2 A cm^{-2} over a 1,000-h operation. Moreover, Fe/Fe$_2$O$_3$ NAs were applied in the electrochemical hydrogenation of various carbonyl compounds to corresponding alcohols with high conversion rates and selectivities.

The catalytic hydrogenation of carbonyl compounds to the corresponding alcohols is one of the most important classes of chemical transformation and is extensively deployed in the manufacture of commodity and fine chemicals and in the refinement of biomass-derived compounds[1–5]. For example, acetone hydrogenation, as a representative carbonyl hydrogenation reaction, is drawing ever-growing attention due to its use in the production of bulk isopropanol, H$_2$ storage, chemical heat pumps, fuel cells and as a model compound for mechanistic studies in biomass transformation[6–9]. Isopropanol has an annual production of more than 3.5 million metric tonnes, and its global demand is growing rapidly, at a rate of ~3% per year[10,11]. At present, catalytic hydrogenation of carbonyl compounds relies primarily on thermocatalysis, particularly in industry (Fig. 1, route 1), and typically proceeds at elevated temperatures (for example, 100–300 °C for thermocatalytic acetone hydrogenation) and under a high-pressure H$_2$ atmosphere,

which results in high energy consumption, high costs and serious safety issues[12–14]. The production of each tonne of H$_2$ via steam reforming releases ~12 tonnes of CO$_2$ (ref. 15). Moreover, the thermocatalysts for the hydrogenation of carbonyl compounds are commonly noble metal-based catalysts (Pt, Pd, Ru, Rh and so on) or flammable Raney Ni (refs. 11,16–20). Accordingly, low-cost, high-performance, mild and carbon-neutral hydrogenation strategies for carbonyl compounds are urgently desired to replace existing energy-intensive and costly thermocatalytic processes.

Electrocatalytic hydrogenation of carbonyl compounds powered by renewable electricity is an appealing alternative, as this not only proceeds at ambient temperature and pressure, but it also utilizes water as the hydrogen source (Fig. 1, route 2)[21,22]. Electrocatalytic carbonyl hydrogenation with Rh-based complexes in organic electrolytes was reported in 1988[23], but it has attracted limited attention and the focus

[1]State Key Laboratory of Solidification Processing and School of Materials Science and Engineering, Northwestern Polytechnical University, Xi'an, P. R. China. [2]Shanghai Key Laboratory of Hydrogen Science & Center of Hydrogen Science, State Key Laboratory of Metal Matrix Composites, School of Materials Science and Engineering, Shanghai Jiao Tong University, Shanghai, P. R. China. [3]Hualu Engineering and Technology Co., Ltd, Xi'an, P. R. China. [4]These authors contributed equally: Jin Lin, Zhenpeng Liu. ✉e-mail: panliu@sjtu.edu.cn; zhangjian@nwpu.edu.cn

Fig. 1 | Routes for the hydrogenation of carbonyl compounds to their corresponding alcohols. Route 1: the traditional thermocatalytic hydrogenation of carbonyl compounds using high-pressure H_2. Route 2: the electrocatalytic hydrogenation of carbonyl compounds using H_2O as the hydrogen source.

has mainly been on the refinement of biomass. For instance, to upgrade the value of biomass-derived chemicals, electrocatalytic hydrogenation of furfural to furfuryl alcohol was developed in aqueous and/or organic electrolytes[24–27]. To understand the mechanism behind the catalytic hydrogenation of biomass-derived carbonyl compounds, the electrocatalytic hydrogenation of acetone and benzaldehyde as probe reactions was investigated with platinum-group metal electrodes[28–32]. Unfortunately, because of the low current densities, strong competition from the hydrogen evolution, carbon–carbon coupling and dehydroxylation reactions, as well as poor stability, the performance of the electrocatalytic hydrogenation of carbonyl compounds has lagged far behind those of thermocatalytic technologies.

In this article we report a high-performance and viable electrocatalytic method for the hydrogenation of carbonyl compounds over economical Fe/Fe$_2$O$_3$ nanoarrays (Fe/Fe$_2$O$_3$ NAs), which have abundant Fe/Fe$_2$O$_3$ interfaces, and where the Fe and Fe$_2$O$_3$ species synergistically enhance the kinetics of carbonyl hydrogenation. With acetone hydrogenation as the probe reaction, in a 1 M KOH aqueous solution containing 20 vol% acetone (2.72 mol l^{-1}), the Fe/Fe$_2$O$_3$ NAs exhibited a very high isopropanol partial current density of 1.6 A cm^{-2} at −0.46 V versus a reversible hydrogen electrode (RHE; without *iR* compensation or ohmic loss compensation), which is substantially higher than the requirement for industrial implementation (>200 mA cm^{-2})[33]. Meanwhile, the Faradaic efficiency (FE$_{isopropanol}$) and selectivity still reached ~80% and ~100%, respectively. In a scaled-up H-type two-electrode alkali electrolyser (100 cm^2) coupled with an anodic oxygen evolution reaction (OER), the Fe/Fe$_2$O$_3$ NAs stably delivered an acetone conversion of >99%, an isopropanol selectivity of ~100% and an isopropanol production rate of 21.6 g g$_{cat}$$^{-1}$ h^{-1} at a large current density of 200 mA cm^{-2} over 1,000 h of operation, which compares well with the <10 g g$_{cat}$$^{-1}$ h^{-1} rates for current thermocatalytic acetone hydrogenation[16,34,35] and propene hydration technologies[10,36,37]. A technoeconomic analysis demonstrated that the production cost of electrocatalytic acetone hydrogenation is approximately US$1,305 per tonne at an electricity price of US$0.03 per kWh, which is lower than the market price of ~US$1,320 per tonne for isopropanol produced via thermocatalytic hydrogenation[10]. Importantly, the Fe/Fe$_2$O$_3$ NAs were universally effective for electrochemical hydrogenations of various carbonyl compounds, including water-soluble ketones and aldehydes, to the corresponding alcohols, with >99% conversion rates and ~100% selectivity. These results reveal the great potential of the electrocatalytic hydrogenation of carbonyl compounds as a next-generation sustainable technology for the production of alcohols.

Results

Synthesis and characterization of Fe/Fe$_2$O$_3$ NAs

Fe/Fe$_2$O$_3$ NAs with abundant Fe/Fe$_2$O$_3$ interfaces were synthesized in a two-step process (Methods and Supplementary Figs. 1 and 2). First, after direct calcination of a commercial Fe foam for 4 h at 450 °C in air, the precursor Fe$_2$O$_3$ NAs were grown on the foam. The morphology and structure of the Fe$_2$O$_3$ NAs on the Fe foam were scrutinized using scanning electron microscopy (SEM), transmission electron microscopy (TEM) and X-ray diffraction (XRD) (Supplementary Figs. 3–5). The Fe$_2$O$_3$ NAs consisted of densely cross-connected nanosheets with thicknesses ranging from 8 to 20 nm. The XRD pattern revealed that a small amount of Fe$_3$O$_4$ was concomitantly formed. During this procedure, the choice of calcination temperature was critical for balancing the crystalline growth and aggregation of the Fe$_2$O$_3$ NAs, and the optimal air-annealing temperature was 450 °C (Supplementary Figs. 6 and 7). Second, the resulting Fe$_2$O$_3$ NAs were electrochemically reduced in a 1 M KOH aqueous solution. Partial Fe$_2$O$_3$ and/or Fe$_3$O$_4$ domains were reduced into metallic Fe, and the Fe/Fe$_2$O$_3$ interfaces were constructed in situ. The current density and time for electrochemical reduction thus played a key role in the fabrication of the Fe/Fe$_2$O$_3$ NAs, and the optimal values were found to be −1.5 A cm^{-2} and 20 min after performance optimization (Supplementary Figs. 8–11).

The XRD pattern for the Fe/Fe$_2$O$_3$ NAs showed peaks distinctive for α-Fe$_2$O$_3$ (JCPDS no. 00-033-0664; Supplementary Fig. 12). As with the precursor Fe$_2$O$_3$ NAs, the characteristic signals for Fe$_3$O$_4$ (220), (400) and (422) facets (JCPDS no. 97-002-0596) appeared at 35.1°, 50.4° and 67.2°, respectively. To exclude the influence of the Fe foam, commercial Fe$_2$O$_3$ nanoparticles (NPs) supported on carbon paper were also used as precursors in constructing Fe/Fe$_2$O$_3$ interfaces through electrochemical reduction (Supplementary Fig. 13). The peaks at 52.4° and 77.2° clearly originated from the (110) and (200) facets of the metallic Fe, respectively (JCPDS no. 00-006-0696; Supplementary Fig. 14). In the X-ray photoelectron spectroscopy (XPS) analysis, the Fe 2*p* peaks for the Fe/Fe$_2$O$_3$ NAs were blueshifted by ~2 eV relative to those for the Fe$_2$O$_3$ NAs, indicating the decreased valence state of the Fe (Supplementary Fig. 15a). Notably, the characteristic signal for Fe^0 at 707.4 eV was observed in the spectrum of the Fe/Fe$_2$O$_3$ NPs (Supplementary Fig. 15b). These spectroscopic results confirmed the formation of metallic Fe^0 through in situ electrochemical reduction of the precursor Fe$_2$O$_3$ NAs. SEM images then showed that the Fe/Fe$_2$O$_3$ NAs retained the morphology of the Fe$_2$O$_3$ NAs on the Fe foam (Fig. 2a and Supplementary Fig. 16). TEM and high-angle annular dark-field scanning TEM (HAADF-STEM) images clearly displayed the lattice fringes with lattice distances of
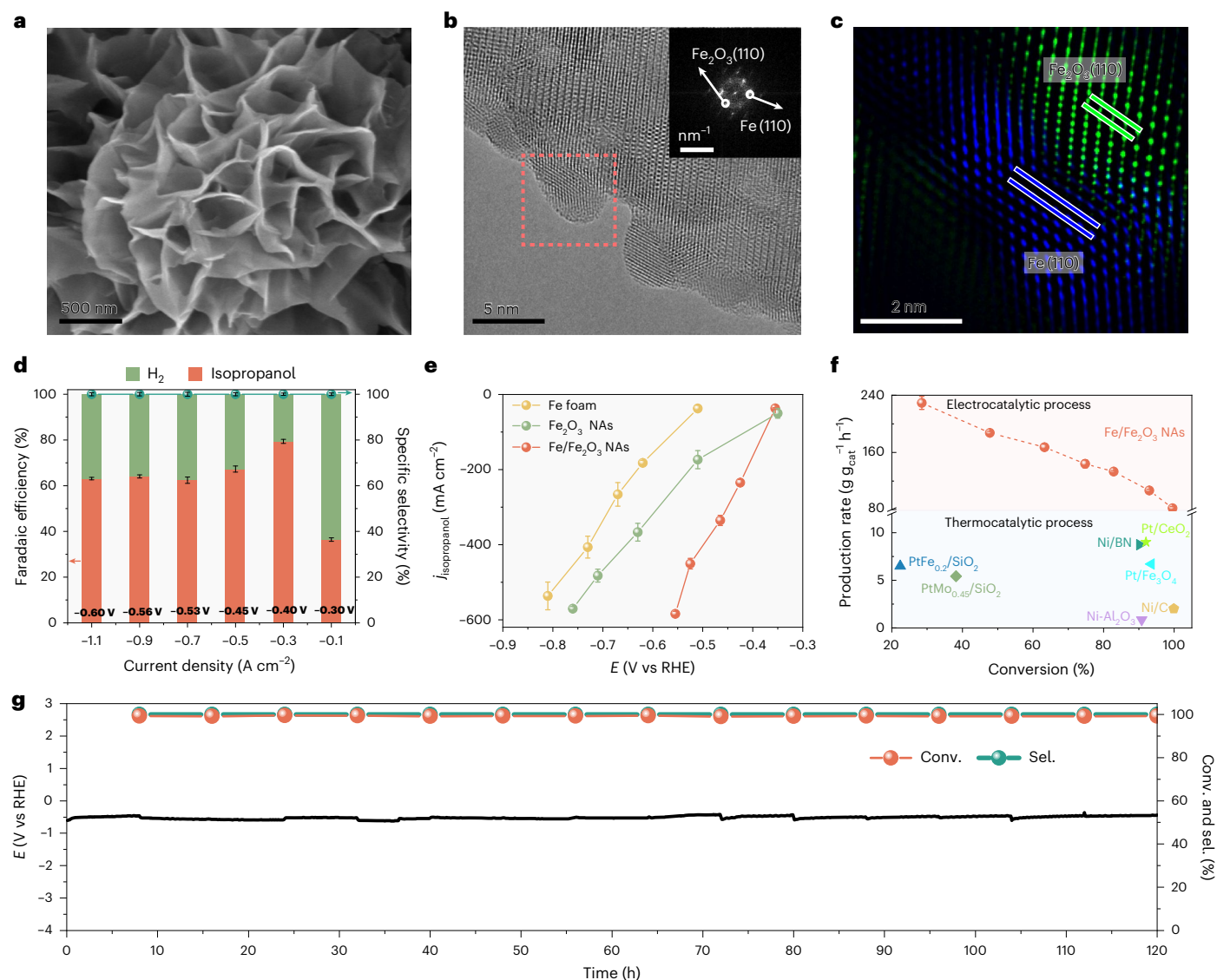
Fig. 2 | Morphology and electrocatalytic performance of catalyst. a, SEM image of Fe/Fe$_2$O$_3$ NAs. **b,c**, HRTEM (**b**) and HAADF-STEM (**c**) images of Fe/Fe$_2$O$_3$ NAs. **d**, Faradaic efficiencies of Fe/Fe$_2$O$_3$ NAs at different current densities. **e**, Isopropanol partial current densities of the Fe foam, Fe$_2$O$_3$ NAs and Fe/Fe$_2$O$_3$ NAs at different potentials. **f**, Comparison of the isopropanol production rate and acetone conversion on the Fe/Fe$_2$O$_3$ NAs with values for previously reported thermocatalysts. **g**, Stability evaluation of the Fe/Fe$_2$O$_3$ NAs over 120 h (15 runs, 8 h for each run) at a current density of −1.0 A cm^{-2}. The electrolyte is 1 M KOH aqueous solution containing 5 vol% acetone. Error bars in **d**–**f** represent the s.d. of three independent measurements. Average (mean) values are presented. Conv., conversion; sel., selectivity.

0.252 and 0.203 nm, which correspond to the Fe$_2$O$_3$ (110) and Fe (110) facets, respectively (Supplementary Fig. 17 and Fig. 2b,c). Clearly, the (110) surface of Fe$_2$O$_3$ and the neighbouring (110) facet of metallic Fe constituted the interfaces in the Fe/Fe$_2$O$_3$ NAs.

Electrocatalytic performance of the Fe/Fe$_2$O$_3$ NAs

For the hydrogenation of carbonyl compounds, the electrocatalytic performance of Fe/Fe$_2$O$_3$ NAs was first investigated in a 1 M KOH aqueous solution in a three-electrode flow cell (Supplementary Figs. 18 and 19). The Hg/HgO and Ni foam served as reference electrode and counter electrode, respectively. The cathodic and anodic chambers were separated by an anion exchange membrane. The potentials given here are referenced to the RHE and have no *iR* correction. As a representative carbonyl compound, acetone was utilized as the probe reactant to evaluate the electrocatalytic hydrogenation performance of the Fe/Fe$_2$O$_3$ NAs. A linear sweep voltammetry (LSV) curve for the Fe/Fe$_2$O$_3$ NAs shows a current density of 29.9 mA cm^{-2} at −0.4 V in 1 M KOH aqueous solution,

which originated completely from the hydrogen evolution reaction (HER; Supplementary Fig. 20). After adding 5 vol% acetone into 1 M KOH aqueous solution, the LSV curve for the Fe/Fe$_2$O$_3$ NAs shifts positively, and the current density increases considerably to 288.8 mA cm^{-2} at −0.4 V, 9.7 times higher than without acetone. This result demonstrates the excellent electrocatalytic activity of Fe/Fe$_2$O$_3$ NAs towards acetone. The gas and liquid products were then analysed using gas chromatography (GC), GC mass spectrometry (GC-MS) and NMR. For electrocatalytic acetone hydrogenation, the GC results indicate that the only gaseous product is H$_2$ (Supplementary Figs. 21 and 22). The GC-MS and NMR analyses verify that isopropanol is the only liquid product, with ~100% selectivity, thus dramatically reducing subsequent costs for isopropanol separation and purification (Supplementary Figs. 22–24). Remarkably, the FE$_{isopropanol}$ and partial current density ($j_{isopropanol}$) for the Fe/Fe$_2$O$_3$ NAs are 79.4% and 234.7 mA cm^{-2} at −0.3 A cm^{-2}, respectively, far higher than the 58.9% and 182.1 mA cm^{-2} for the Fe foam and 53.6% and 173.5 mA cm^{-2} for the Fe$_2$O$_3$ NAs (Fig. 2d,e and Supplementary

Figs. 25 and 26). The Fe/Fe$_2$O$_3$ NAs exhibit a substantially lower onset overpotential of ~484 mV, in comparison with ~590 mV for Fe$_2$O$_3$ NAs and ~656 mV for Fe foam (Supplementary Fig. 27a). The related Tafel slope of the Fe/Fe$_2$O$_3$ NAs is ~89.9 mV dec^{-1}, which is considerably lower than the ~130.8 mV dec^{-1} for Fe$_2$O$_3$ NAs and ~167.9 mV dec^{-1} for Fe foam (Supplementary Fig. 27b), indicating accelerated reaction kinetics for electrocatalytic acetone hydrogenation. In addition, the electrochemical active surface area (ECSA)-normalized LSV curves and $j_{isopropanol}$ show that the Fe/Fe$_2$O$_3$ NAs have higher intrinsic activity than the Fe$_2$O$_3$ NAs and Fe foam (Supplementary Figs. 28 and 29). Even at a particularly high current density of −1.1 A cm^{-2}, FE$_{isopropanol}$ and $j_{isopropanol}$ for the Fe/Fe$_2$O$_3$ NAs still reaches 63.1% and 694.2 mA cm^{-2}, respectively, far larger than the industrially required current density of 200 mA cm^{-2}. At an acetone conversion of ~99.9%, the isopropanol selectivity remains at ~100% (Supplementary Fig. 30). As shown in Fig. 2f and Supplementary Fig. 31, even at an acetone conversion of 99.9%, the isopropanol production rate of the Fe/Fe$_2$O$_3$ NAs at −1.3 A cm^{-2} reaches 83.3 g g$_{cat}^{-1}$ h^{-1}, which is drastically higher than the values for state-of-the-art thermocatalysts in acetone hydrogenation, such as 9.1 g g$_{cat}^{-1}$ h^{-1} for Pt/CeO$_2$ (ref. 34), 9.0 g g$_{cat}^{-1}$ h^{-1} for Ni/BN (ref. 35), 7.1 g g$_{cat}^{-1}$ h^{-1} for Pt/Fe$_3$O$_4$ (ref. 16) and 6.6 g g$_{cat}^{-1}$ h^{-1} for PtMo$_{0.45}$/SiO$_2$ (ref. 17), and in propene hydration, for example, 0.12 g g$_{cat}^{-1}$ h^{-1} for H-zeolite beta[36] and 0.089 g g$_{cat}^{-1}$ h^{-1} for HPW/SiO$_2$ (ref. 37).

Electrocatalytic stability is another key parameter for evaluating electrocatalyst performance. Accordingly, a recycling experiment for electrocatalytic acetone hydrogenation on Fe/Fe$_2$O$_3$ NAs was conducted at a large current density of −1.0 A cm^{-2} in a three-electrode flow cell. As shown in Fig. 2g, owing to the excellent electrocatalytic performance of the Fe/Fe$_2$O$_3$ NAs, 0.79 g of acetone in 20 ml of 1 M KOH solution (5 vol%) was efficiently hydrogenated into 0.786 g of isopropanol after the first electrocatalysis run (8 h per run), corresponding to an acetone conversion of ~99% and an isopropanol selectivity of ~100%. With increased recycling runs (120 h for 15 runs), the acetone conversion and isopropanol selectivity of the Fe/Fe$_2$O$_3$ NAs remained stable at ≥99% and ~100%, respectively. Meanwhile, the recycling rate of the Fe/Fe$_2$O$_3$ NAs remained stable at ~99%, and the output isopropanol concentration over the Fe/Fe$_2$O$_3$ NAs remained good for each recycling run (Supplementary Figs. 32 and 33). The increases in the applied potentials were negligible. SEM, XRD and XPS characterizations showed no obvious morphological or structural changes for the Fe/Fe$_2$O$_3$ NAs after a long-term electrocatalytic stability test (Supplementary Figs. 34–36).

To investigate the universality of the electrocatalytic hydrogenation strategy for various carbonyl compounds, the electrocatalytic performance of the Fe/Fe$_2$O$_3$ NAs was evaluated in a three-electrode flow cell. 1 M KOH aqueous solutions containing 1 vol% carbonyl compounds, including water-soluble ketones and aldehydes, were used as electrolytes. As shown in Fig. 3 and Supplementary Figs. 37–41, the Fe/Fe$_2$O$_3$ NAs delivered high electrocatalytic conversions of ≥99% for various carbonyl compounds, as well as alcohol selectivities of ~100%. The ^{1}H NMR spectra of the resulting alcohols are shown in Supplementary Figs. 42–61. To assess the feasibility of industrial implementation, two typical two-electrode electrolysers, a single-pass flow electrolyser with an electrode area of 25 cm^2 and an H-type batch electrolyser with an electrode area of 100 cm^2, were operated for electrocatalytic acetone hydrogenation (Supplementary Figs. 62 and 63). NiFe layered double hydroxides (NiFe-LDH) on Ni foam served as the anode for the OER (Supplementary Fig. 64). In the single-pass flow electrolyser, 1 M KOH electrolyte containing 1 vol% acetone was continuously fed into the cathodic Fe/Fe$_2$O$_3$ NAs. Notably, the Fe/Fe$_2$O$_3$ NAs exhibited an acetone conversion of ~94% and an isopropanol selectivity of ~100% at an applied current density of 200 mA cm^{-2} and a flow rate of 40 ml h^{-1} (Fig. 4a). Over a 90-h operation at 200 mA cm^{-2}, the Fe/Fe$_2$O$_3$ NAs stably achieved an acetone conversion of ~92% and an isopropanol selectivity of ~100%, corresponding to a continuous isopropanol production rate of 4.1 g g$_{cat}^{-1}$ h^{-1} (Fig. 4b). Benefiting from high conversion rates
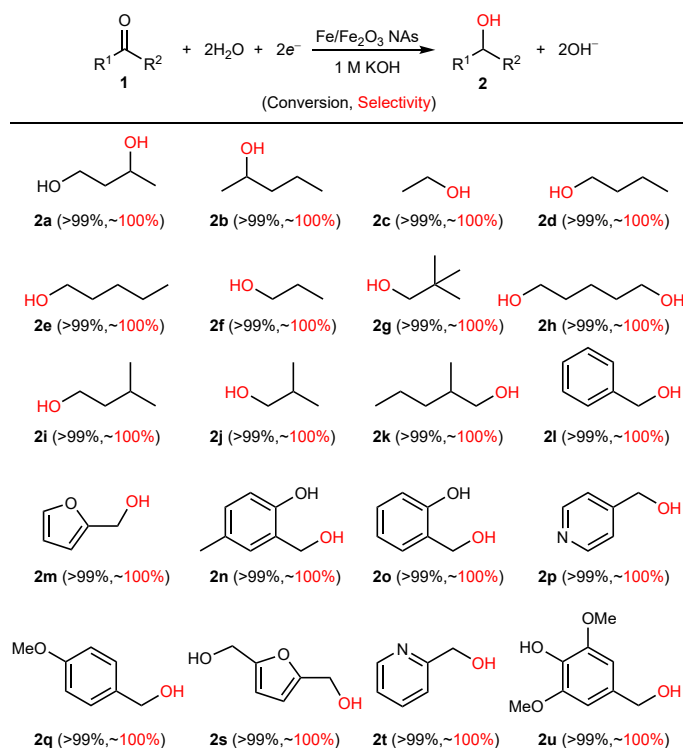

Fig. 3 | Substrate scope of electrocatalytic hydrogenation. Carbonyl compounds are electrochemically hydrogenated at 1.0 A cm^{-2} for 2 h, except for **2a** and **2b** (5 h). Reaction conditions: 20 ml of 1 M KOH aqueous solution, 1 vol% carbonyl compounds, 1.0 cm^2 Fe/Fe$_2$O$_3$ NAs, room temperature. Three independent measurements were carried out, and average values are presented.

and selectivities, the high concentrations of products could substantially reduce the cost of subsequent energy-intensive separation and purification. When the acetone concentration was larger than 10 vol%, the resulting concentrated isopropanol gradually penetrated into the anodic chamber during long-term electrolysis. Therefore, 1 l of 1 M KOH aqueous solution containing 10 vol% acetone was used as the cathodic electrolyte in the H-type batch electrolyser. In the first cycle (12 h), the Fe/Fe$_2$O$_3$ NAs showed a very high acetone conversion of ~99% with an isopropanol selectivity of ~100% at 200 mA cm^{-2}. Importantly, over a 1,000-h stability test at 200 mA cm^{-2}, the Fe/Fe$_2$O$_3$ NAs exhibited a steady acetone conversion of ~99%, an isopropanol selectivity of ~100% and an isopropanol production rate of 21.6 g g$_{cat}^{-1}$ h^{-1}, which is considerably higher than the <10 g g$_{cat}^{-1}$ h^{-1} for current thermocatalytic technologies (Fig. 4c). As displayed in Fig. 4d, Supplementary Figs. 65 and 66 and Supplementary Video 1, under irradiation with natural sunlight, a commercial solar panel (1.45 m^2) with an output voltage of 7.85 V and a power density of 35.3 W stably powered three tandem H-type batch electrolysers for electrocatalytic acetone hydrogenation. After simple distillation and dehydration, 1 l of isopropanol (785.5 g) with a purity of 99.7% was eventually achieved (Fig. 4e, Supplementary Figs. 67 and 68, Supplementary Table 1 and Supplementary Video 2). Furthermore, a technoeconomic analysis for electrocatalytic acetone hydrogenation was conducted using a reported model[38–41], which included the costs of capital, maintenance, installation, input materials and operation (Supplementary Fig. 69, Supplementary Table 2 and Supplementary Note 5). Under the operating conditions (200 mA cm^{-2} and FE$_{isopropanol}$ = 50%), the cost of the electrocatalytic acetone hydrogenation process was calculated to be ~US$1,305 per tonne of isopropanol at a given electricity price of US$0.03 per kWh, which is lower than the US$1,320 per tonne market price of isopropanol achieved by thermocatalytic hydrogenation. Notably, the electrochemical acetone
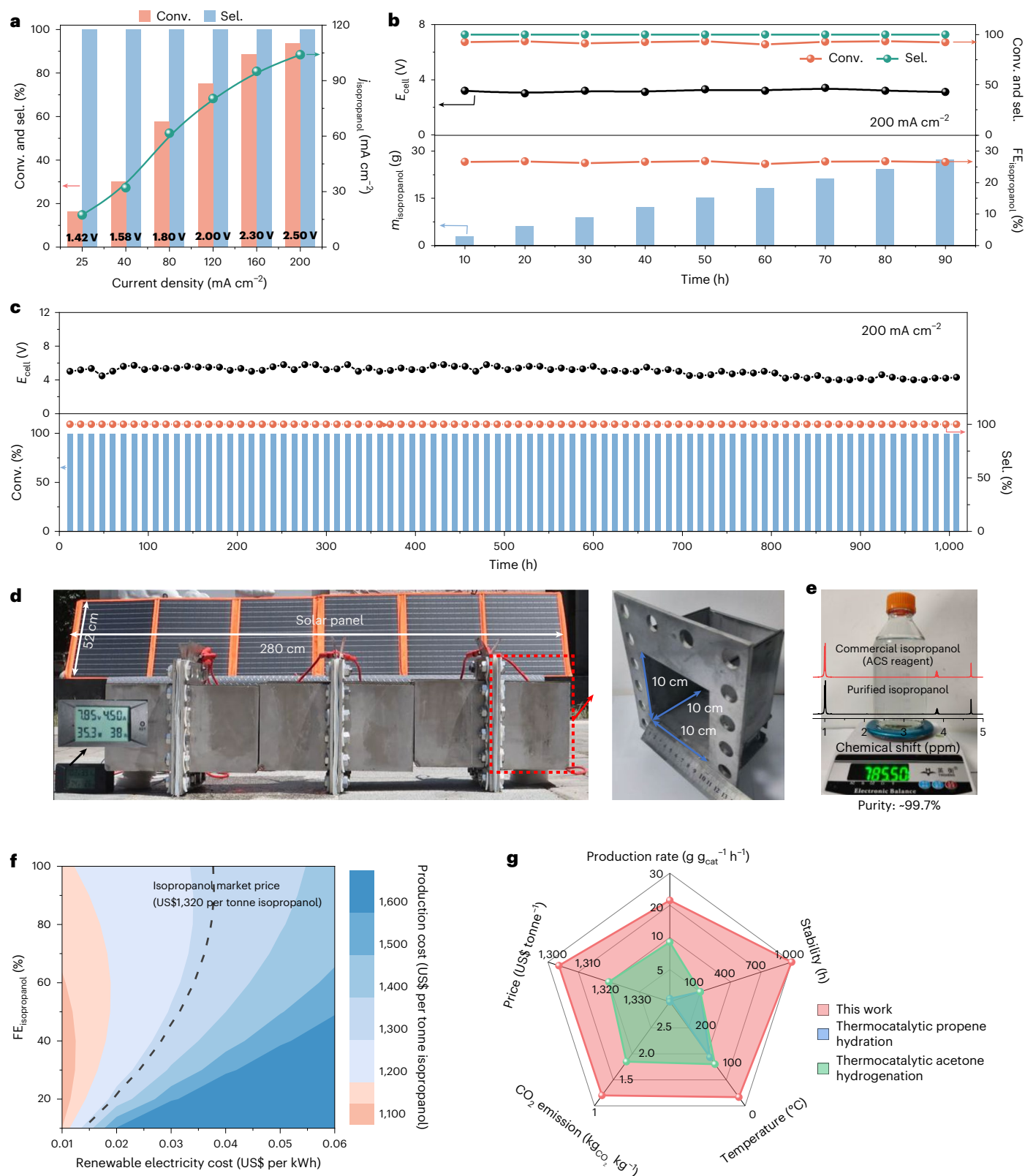
Fig. 4 | Electrocatalytic performance in large-area two-electrode electrolysers. a, Single-pass acetone conversion, isopropanol selectivity, cell voltage and partial current density at different current densities in the single-pass flow electrolyser. **b**, Continuous 90-h production of isopropanol at a current density of 200 mA cm^{-2} by feeding 1 M KOH aqueous solution containing 1 vol% acetone at a flow rate of 40 ml h^{-1} into the single-pass flow electrolyser. m, amount of product. **c**, Stability evaluation of the Fe/Fe$_2$O$_3$ NAs at a current density of 200 mA cm^{-2} in the H-type batch electrolyser. **d**, Photographs of three tandem H-type batch electrolysers powered by a large solar panel. **e**, Photograph and

^{1}H NMR spectra of as-produced high-purity isopropanol (~1 l) after distillation and dehydration. **f**, A contour map for the total isopropanol production costs via the electrocatalytic hydrogenation process at 200 mA cm^{-2} with respect to the different FEs of isopropanol and renewable electricity costs. The dashed line represents the isopropanol market price (US$1,320 per tonne isopropanol). **g**, A radar plot comparison of electrocatalytic and thermocatalytic acetone hydrogenation and propene hydration, including production rate, stability, operating temperature, CO$_2$ emission and production price.
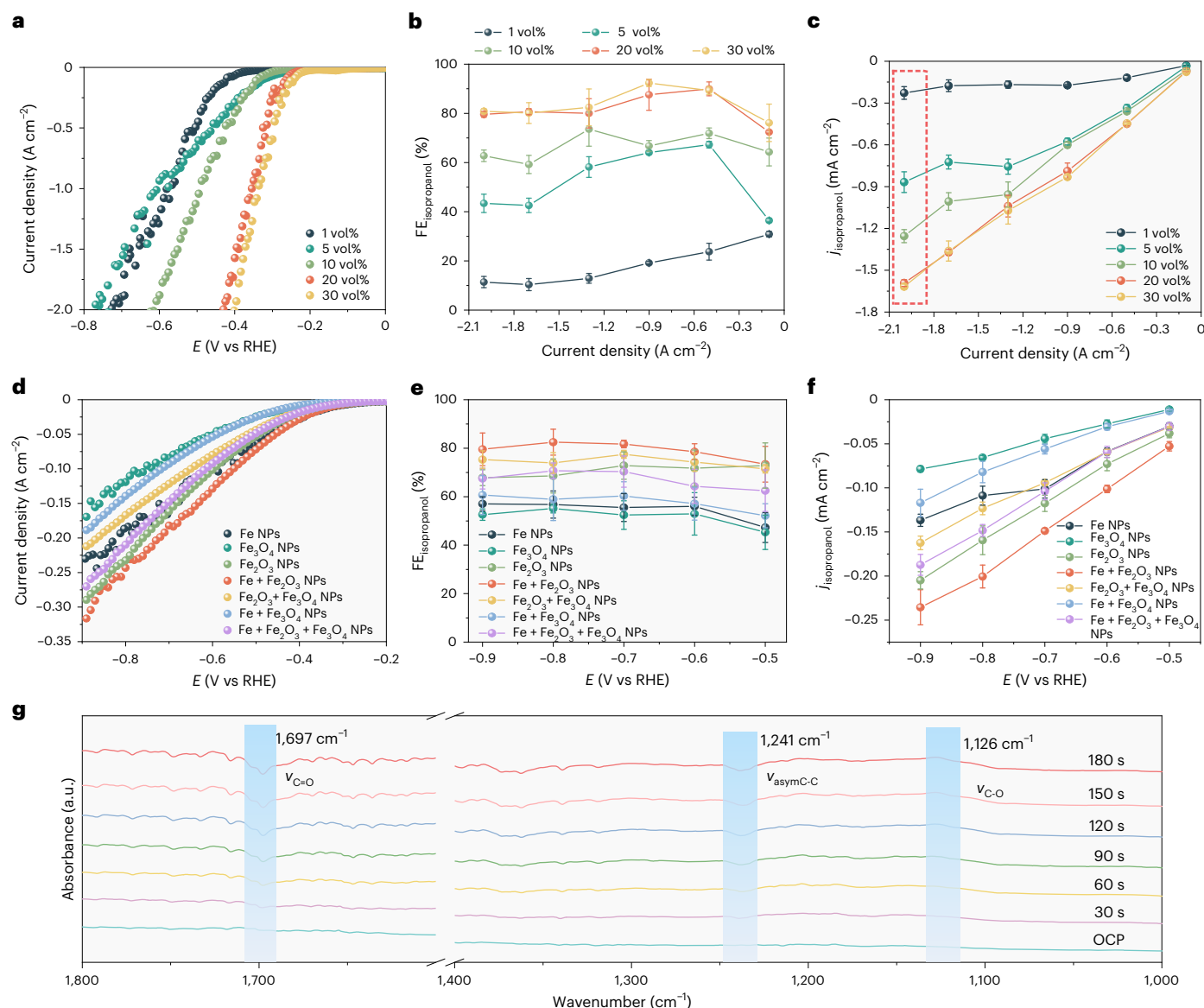
Fig. 5 | Mechanistic investigation of electrocatalytic acetone hydrogenation.
a–c, Polarization curves (**a**), FE$_{isopropanol}$ (**b**) and $j_{isopropanol}$ (**c**) for Fe/Fe$_2$O$_3$ NAs in 1 M KOH aqueous solution containing different amounts of acetone. **d–f**, Polarization curves (**d**), FE$_{isopropanol}$ (**e**) and $j_{isopropanol}$ (**f**) for commercial Fe NPs, Fe$_2$O$_3$ NPs, Fe$_3$O$_4$ NPs, Fe + Fe$_2$O$_3$ NPs, Fe + Fe$_3$O$_4$ NPs, Fe$_2$O$_3$ + Fe$_3$O$_4$ NPs and Fe + Fe$_2$O$_3$ + Fe$_3$O$_4$ NPs.

g, In situ electrochemical ATR-FTIR spectra during electrocatalytic acetone hydrogenation on Fe/Fe$_2$O$_3$ NAs. OCP, open-circuit potential. Error bars in **b**, **c**, **e**, **f** represent s.d. of three independent measurements. Average (mean) values are presented.

hydrogenation was profitable when FE$_{isopropanol}$ was >40% (Fig. 4f). As shown in Fig. 4g, these results clearly demonstrate the potential of electrocatalytic technology to replace the traditional thermocatalytic hydrogenation processes used in producing alcohols from the corresponding carbonyl compounds.

Mechanistic study of electrocatalytic acetone hydrogenation
Isotopic labelling analyses were carried out to identify the hydrogen source for the electrocatalytic acetone hydrogenation. A 1 M KOH D$_2$O solution containing 5 vol% acetone was used as the electrolyte. After electrocatalytic acetone hydrogenation on the Fe/Fe$_2$O$_3$ NAs, GC-MS analyses were conducted. The characteristic mass fragmentation pattern for C$_3$D$_8$O was detected at an m/z of 66, confirming that water was the hydrogen source for the electrochemical acetone hydrogenation (Supplementary Fig. 70).

To unveil the competition between acetone hydrogenation and the HER, the influences of acetone concentration on electrocatalytic

activity and selectivity were further studied in 1 M KOH aqueous solution. As the acetone concentration increased from 1 vol% to 30 vol%, the polarization curve for the Fe/Fe$_2$O$_3$ NAs drastically shifted to lower potentials, and FE$_{isopropanol}$ noticeably increased from ~11.4% to ~80.9% at −2.0 A cm^{-2} (Fig. 5a,b). In 1 M KOH solution containing 1 vol% acetone, as the current density increased, FE$_{isopropanol}$ of the Fe/Fe$_2$O$_3$ NAs gradually decreased from ~30.9% at −0.1 A cm^{-2} to ~11.4% at −2 A cm^{-2} as a result of growing competition with the HER. In comparison, at high acetone concentrations (≥5 vol%), FE$_{isopropanol}$ of the Fe/Fe$_2$O$_3$ NAs initially improved and subsequently declined as the current density increased. This is because FE$_{isopropanol}$ is synergistically influenced by the acetone hydrogenation kinetics, the competitive HER, and mass transfer of acetone (Supplementary Figs. 71–73). Notably, in 1 M KOH solution containing 20 vol% acetone, $j_{isopropanol}$ was as large as 1.6 A cm^{-2} at −2 A cm^{-2}, far higher than the 1.2 A cm^{-2} for 10 vol% acetone concentration, 0.8 A cm^{-2} for 5 vol% acetone concentration and 0.2 A cm^{-2} for 1 vol% acetone concentration (Fig. 5c). These results indicate that the

electrocatalytic activity for acetone hydrogenation on Fe/Fe$_2$O$_3$ NAs intrinsically surpasses that of the competitive HER.

The Fe/Fe$_2$O$_3$ NAs were composed of metallic Fe^0, Fe$_2$O$_3$ and Fe$_3$O$_4$ species. To identify the active centres of the Fe/Fe$_2$O$_3$ NAs for acetone hydrogenation, the electrocatalytic performance of commercial metallic Fe^0 NPs (Fe NPs), Fe$_2$O$_3$ NPs, Fe$_3$O$_4$ NPs and physically mixed catalysts (Fe + Fe$_2$O$_3$ NPs, Fe$_2$O$_3$ + Fe$_3$O$_4$ NPs, Fe + Fe$_3$O$_4$ NPs and Fe + Fe$_2$O$_3$ + Fe$_3$O$_4$ NPs) were systematically evaluated in 1 M KOH electrolyte containing 5 vol% acetone. As shown in Fig. 5d–f, FE$_\text{isopropanol}$ and $j_\text{isopropanol}$ of the commercial Fe$_2$O$_3$ NPs were ~68.6% and 159.4 mA cm^{-2} at −0.8 V, much higher than the ~56.7% and 108.8 mA cm^{-2} for commercial Fe NPs and ~55.1% and 65.7 mA cm^{-2} for Fe$_3$O$_4$ NPs. After physical mixing with the Fe$_3$O$_4$ NPs, $j_\text{isopropanol}$ of the as-achieved Fe$_2$O$_3$ + Fe$_3$O$_4$ NPs, and Fe + Fe$_2$O$_3$ + Fe$_3$O$_4$ NPs substantially decreased to 123.2 mA cm^{-2} and 148.3 mA cm^{-2}, respectively. In contrast, the Fe + Fe$_2$O$_3$ NPs had an FE$_\text{isopropanol}$ of ~82.5% and $j_\text{isopropanol}$ of 200.6 mA cm^{-2} at −0.8 V, which are considerably higher than the values for bare Fe NPs and Fe$_2$O$_3$ NPs. Furthermore, the ECSA-normalized LSVs and $j_\text{isopropanol}$ values of different commercial NPs revealed that the Fe + Fe$_2$O$_3$ NPs presented the highest intrinsic activity (Supplementary Figs. 74–76). These results confirm that the synergistic effects of the metallic Fe^0 and Fe$_2$O$_3$ in the Fe/Fe$_2$O$_3$ NAs play a crucial role in electrocatalytic acetone hydrogenation.

Typically, pH plays a major role in determining hydrogenation and HER kinetics. Several aqueous solutions with different pH values were used as electrolytes containing 5 vol% acetone. At an applied current density of −0.5 A cm^{-2}, FE$_\text{isopropanol}$ of the Fe/Fe$_2$O$_3$ NAs in 1 M KHCO$_3$ solution (pH 8.5) drastically decreased to ~4.5% from ~69.7% in 1 M KOH solution, leading to an extremely low $j_\text{isopropanol}$ of only 0.023 A cm^{-2} (Supplementary Fig. 77). When the concentration of the KOH solution was gradually increased from 0.5 to 3 M, the $j_\text{isopropanol}$ plot shifted to lower potentials. Cyclic voltammograms (CVs) were generated to understand the influence of active H* on acetone hydrogenation. As described in Supplementary Figs. 78 and 79, the CV curve for commercial Fe$_2$O$_3$ NPs in 1 M KOH solution showed an anodic peak at ~0.32 V versus RHE, which was assigned to the desorption of surface H*. After adding acetone into the 1 M KOH solution, the peak intensity for H* desorption from the Fe$_2$O$_3$ NPs was not obviously affected by the acetone concentration. When the Fe$_2$O$_3$ NPs were electrochemically reduced to Fe/Fe$_2$O$_3$ NPs, the intensity of H* desorption substantially increased (by 7.58 times) in 1 M KOH solution. Additionally, the peak for H* desorption shifted positively to ~0.47 V versus RHE, implying greatly accelerated water dissociation for H* production. Along with the increased acetone concentration, the intensity of H* desorption from the Fe/Fe$_2$O$_3$ NPs sharply declined, consistent with that for commercial Fe NPs. This was attributed to strong competition from acetone adsorption or the consumption of active H*. These results suggest that metallic Fe^0 species provide active centres for acetone adsorption and that both the Fe^0 and Fe$_2$O$_3$ species are active in the formation of active H*, which synergistically promotes electrocatalytic acetone hydrogenation.

In situ electrochemical attenuated total reflectance–Fourier transform infrared (ATR-FTIR) spectroscopy was conducted to probe the underlying electrocatalytic mechanism for acetone hydrogenation. The in situ electrochemical ATR-FTIR spectra were recorded at −20 mA cm^{-2} (Fig. 5g and Supplementary Fig. 80). Notably, during the electrocatalytic process, the characteristic peak for C=O bonds at 1,697 cm^{-1} gradually weakened, while the peak for the C−O bonds intensified, indicating acetone hydrogenation to isopropanol. These results demonstrate the occurrence of acetone hydrogenation.

Conclusions

We have demonstrated a high-performance electrocatalytic strategy for hydrogenating carbonyl compounds into the corresponding alcohols under ambient conditions. The synergistic effects of the Fe and Fe$_2$O$_3$ species are inherently responsible for the high activity and selectivity of the Fe/Fe$_2$O$_3$ NAs. Due to the ampere-level current density, near-unity selectivity, 1,000-h long-term stability, broad applicability, low cost and sustainability, the electrocatalytic hydrogenation of carbonyl compounds holds great potential for competing against current energy-intensive and costly high-pressure H$_2$-based thermocatalytic technologies.

Methods

Synthesis of Fe$_2$O$_3$ NAs and Fe/Fe$_2$O$_3$ NAs

The Fe/Fe$_2$O$_3$ NAs on commercial Fe foam were synthesized by means of thermal oxidation and in situ electroreduction processes. Specifically, a piece of commercial Fe foam (1.0 × 3.0 cm^2) was consecutively cleaned by using 1 M HCl solution, acetone, ethanol and deionized water, and eventually dried in a N$_2$ atmosphere. Subsequently, the Fe foam was annealed for 4 h at different temperatures (350 °C, 450 °C, 550 °C) in air to form Fe$_2$O$_3$ NAs. Afterwards, the Fe$_2$O$_3$ NAs were electrochemically reduced into Fe/Fe$_2$O$_3$ NAs in 1 M KOH aqueous solution at different current densities (−1.0 A cm^{-2}, −1.5 A cm^{-2} and −2.0 A cm^{-2}) for various durations (10 min, 20 min, 30 min and 40 min), using a Hg/HgO electrode and Ni foam as the reference and counter electrodes, respectively. The loading weight of Fe/Fe$_2$O$_3$ NAs on the Fe foam was estimated to be 3.0 mg cm^{-2} (Supplementary Fig. 81 and Supplementary Note 10). With a two-electrode flow electrolyser with a large electrode area of 25 cm^2 (5 × 5 cm^2), Fe/Fe$_2$O$_3$ NAs were synesized in the same way, except for the electroreduction current density (−200 mA cm^{-2}) and time (150 min). For the two-electrode H-type electrolyser with a large electrode area of 100 cm^2 (10 × 10 cm^2), the Fe/Fe$_2$O$_3$ NAs were fabricated in the same way, except for the electroreduction current density (−200 mA cm^{-2}) and time (150 min).

Fabrication of the cathode with commercial NPs

To prepare the catalyst ink, 15 mg of commercial NPs, 950 µl of isopropanol and 50 µl of Nafion solution (5 wt%) were mixed. After 30 min of sonication, a well-dispersed catalyst ink was achieved. For the catalyst ink, the molar ratio of two mixed NPs was 1:1. For the ink of mixed Fe NPs, Fe$_2$O$_3$ NPs and Fe$_3$O$_4$ NPs, the molar ratio was 1:1:1. Eventually, the dispersed catalyst ink was sprayed onto carbon paper to serve as the cathode, with a catalyst loading weight of ~1 mg cm^{-2}.

Synthesis of the NiFe-LDH nanosheets

NiFe-LDH on Ni foam was synthesized by means of a simple electrodeposition method. Specifically, commercial Ni foam (1 × 3 cm^2) with a thickness of 1.6 mm was consecutively cleaned using 1 M HCl solution, acetone and ethanol, rinsed with distilled water, and eventually dried with nitrogen flow. Subsequently, the Ni foam was immersed in an aqueous solution containing 0.12 M Ni(NO$_3$)$_2$·6H$_2$O and 0.12 M FeSO$_4$·7H$_2$O. With a Pt plate as counter electrode and Ag/AgCl as reference electrode, electrodeposition was performed in the above solution at −10 mA cm^{-2} for 6 min. Eventually, NiFe-LDH on Ni foam was obtained after washing with deionized water and drying in an oven.

Electrocatalytic evolution

Electrocatalytic performance was assessed in a three-electrode electrolyser. The three-electrode electrolyser with a window area of 1 × 1 cm^2 was assembled with gaskets and anode and cathode flow-field plates. The anode and cathode plates were separated by an anion exchange membrane (Fumasep FAB-PK-130) and were individually supplied with electrolyte. The catholyte was 1 M KOH aqueous solution containing different concentrations of acetone, and the anolyte was 1 M KOH aqueous solution. The flow rate of the cathode and anode electrolytes was 235 ml min^{-1}. For standard tests, a Hg/HgO (in KOH electrolyte) electrode and Ni foam were used as the reference and counter electrodes, respectively. Prepared Fe/Fe$_2$O$_3$ NAs served as the working electrode. Polarization curves were recorded at a scan rate of 1 mV s^{-1}. The stability test was conducted at a current density of −1.0 A cm^{-2}. In detail, after electrocatalytic hydrogenation for 8 h, the acetone was

mostly hydrogenated into isopropanol, which was denoted as one recycling run. Subsequently, a fresh 20-ml 1 M KOH solution containing 5 vol% acetone was directly fed to the flow cell for the next recycling run without disassembling. For electrochemical tests, all potentials were calibrated versus RHE, $E_{RHE} = E_{Hg/HgO} + 0.098\ V + 0.059\ V \times pH$. All potentials were without *iR* correction.

Two-electrode tests under industrial conditions were performed in a single-pass flow electrolyser ($5 \times 5\ cm^2$) and an H-type batch electrolyser ($10 \times 10\ cm^2$). The Fe/Fe_2O_3 NAs and NiFe-LDH on Ni foam were used as cathode and anode, respectively. In the flow electrolysers, the electrolyte was pumped to the cathode at a flow rate of 40 ml min^{-1}.

Product analyses
Chronopotentiometry experiments were conducted at current densities of −0.1, −0.3, −0.5, −0.7, −0.9, −1.1 and −1.3 A cm^{-2} to evaluate the FE and selectivity of the Fe/Fe_2O_3 NAs. At each current density, electrolysis was carried out for 600 s to collect products. The gaseous products were analysed by GC (Fuli GC7900 Instruments) with a thermal conductivity detector and a flame ionization detector. For qualitative and quantitative analyses of the liquid products, 500 μl of electrolyte containing the products was neutralized with 0.5 M H_2SO_4 aqueous solution. The solution was directly injected into a GC set-up (Fuli GC9790Plus Instruments) equipped with a flame ionization detector. The liquid products were further identified by ^{1}H NMR. After electrocatalytic hydrogenation, the electrolyte was neutralized with 0.5 M H_2SO_4 aqueous solution; then 500 μl of the above solution was mixed with 200 μl of D_2O for NMR analyses. The FE of the products was calculated based on the following equation:

$$FE(\%) = \frac{n \times m \times F}{It} \times 10 \qquad (1)$$

where *n* is the number of transferred electrons, *m* is the amount of product, F is the Faraday constant, *I* is the total current density and *t* is the electrolysis time.

The conversion of carbonyl compounds was determined according to

$$Conversion(\%) = \frac{C_{carbonyl}^0 - C_{carbonyl}^1}{C_{carbonyl}^0} \times 100 \qquad (2)$$

where $C_{carbonyl}^0$ and $C_{carbonyl}^1$ are the carbonyl compound concentrations before and after electrocatalytic hydrogenation, respectively.

The selectivity of alcohols was achieved according to

$$Selectivity(\%) = \frac{C_{alcohol}^1}{C_{carbonyl}^0 - C_{carbonyl}^1} \times 100 \qquad (3)$$

where $C_{alcohol}^1$ is the concentration of alcohols after electrocatalytic hydrogenation.

The production rate of isopropanol was calculated as

$$Production\ rate\ of\ isopropanol\ \left(g\ g_{cat}^{-1}\ h^{-1}\right) = \frac{C \times V}{m \times t} \qquad (4)$$

where *C* is the concentration of isopropanol after electrocatalytic concentration, *V* is the volume of electrolyte, *m* is the mass of the Fe/Fe_2O_3 NAs on Fe foam, and *t* is the time of electrocatalytic hydrogenation.

Characterizations
SEM images were acquired using an FEI-Verios G4 field-emission scanning electron microscope. TEM images and related elemental mapping images for Fe/Fe_2O_3 NAs were obtained on an FEI Titan Themis aberration-corrected transmission electron microscope at 300 kV. XPS measurements were conducted on a Kratos-Axis Supra spectrometer using monochromatic Al Kα radiation (1,486.6 eV) and a low-energy flood gun as neutralizer. All XPS spectra were calibrated by aligning the detected carbon C 1*s* peak to 284.6 eV. XRD patterns were recorded using an X-ray diffractometer (Panalytical BV) with Cu Kα radiation. NMR spectra were obtained on a Bruker Avance III HD 400-MHz spectrometer using diluted dimethyl sulfoxide in D_2O as an internal standard. GC-MS spectra were taken using an Agilent 8890-7000D mass spectrometer coupled with an Agilent Technologies 8860 GC system. A Nicolet-is50 spectrometer equipped with an MCT-A detector was used for ATR-FTIR measurements. Fe/Fe_2O_3 NAs were pressed onto a Si prism using a glassy carbon electrode to serve as the working electrode. The Hg/HgO and PT electrodes served as reference and counter electrodes, respectively. The electrolyte was 1 M KOH aqueous solution containing 5 vol% acetone. Data acquisition was conducted in the range of 4,000–650 cm^{-1} with a nominal resolution of 4 cm^{-1}. The electrode settings and reaction conditions were consistent with those for electrocatalytic experiments.

Data availability
The data supporting the finding of this work are available in the main text and Supplementary Information. Additional data related to this work may be requested from the corresponding authors. Source data are provided with this paper.

References
1. Zhang, F.-H., Zhang, F.-J., Li, M.-L., Xie, J.-H. & Zhou, Q.-L. Enantioselective hydrogenation of dialkyl ketones. *Nat. Catal.* **3**, 621–627 (2020).
2. Zhou, H. et al. Organocatalytic stereoselective cyanosilylation of small ketones. *Nature* **605**, 84–89 (2022).
3. Zhao, M. et al. Metal–organic frameworks as selectivity regulators for hydrogenation reactions. *Nature* **539**, 76–80 (2016).
4. Liu, P. et al. Photochemical route for synthesizing atomically dispersed palladium catalysts. *Science* **352**, 797–800 (2016).
5. Bordet, A. et al. Selectivity control in hydrogenation through adaptive catalysis using ruthenium nanoparticles on a CO_2-responsive support. *Nat. Chem.* **13**, 916–922 (2021).
6. Ozkar, S. & Finke, R. G. Iridium(0) nanocluster, acid-assisted catalysis of neat acetone hydrogenation at room temperature: exceptional activity, catalyst lifetime and selectivity at complete conversion. *J. Am. Chem. Soc.* **127**, 4800–4808 (2005).
7. Wang, X. S., Jiao, Y., Li, L. Q., Zheng, Y. & Qiao, S. Z. Local environment determined reactant adsorption configuration for enhanced electrocatalytic acetone hydrogenation to propane. *Angew. Chem. Int. Ed.* **61**, e202114253 (2022).
8. Waldie, K. M., Flajslik, K. R., McLoughlin, E., Chidsey, C. E. D. & Waymouth, R. M. Electrocatalytic alcohol oxidation with ruthenium transfer hydrogenation catalysts. *J. Am. Chem. Soc.* **139**, 738–748 (2017).
9. Feng, R. et al. Reversible ketone hydrogenation and dehydrogenation for aqueous organic redox flow batteries. *Science* **372**, 836–840 (2021).
10. Panjapakkul, W. & El-Halwagi, M. M. Technoeconomic analysis of alternative pathways of isopropanol production. *ACS Sustain. Chem. Eng.* **6**, 10260–10272 (2018).
11. Shen, M. et al. Ni-foam-structured Ni-Al_2O_3 ensemble as an efficient catalyst for gas-phase acetone hydrogenation to isopropanol. *ACS Appl. Mater. Interfaces* **13**, 28334–28347 (2021).
12. Rahman, A. Catalytic hydrogenation of acetone to isopropanol: an environmentally benign approach. *Bull. Chem. React. Eng.* **5**, 113–126 (2010).

13. Meng, N., Shinoda, S. & Saito, Y. Improvements on thermal efficiency of chemical heat pump involving the reaction couple of 2-propanol dehydrogenation and acetone hydrogenation. *Int. J. Hydrogen Energ.* **22**, 361–367 (1997).

14. Balouch, A., Ali Umar, A., Shah, A. A., Mat Salleh, M. & Oyama, M. Efficient heterogeneous catalytic hydrogenation of acetone to isopropanol on semihollow and porous palladium nanocatalyst. *ACS Appl. Mater. Interfaces* **5**, 9843–9849 (2013).

15. Zhu, Q. et al. Enhanced CO_2 utilization in dry reforming of methane achieved through nickel-mediated hydrogen spillover in zeolite crystals. *Nat. Catal.* **5**, 1030–1037 (2022).

16. Ji, Y. et al. Porous bimetallic Pt-Fe nanocatalysts for highly efficient hydrogenation of acetone. *Nano Res.* **8**, 2706–2713 (2015).

17. Ro, I. et al. Intrinsic activity of interfacial sites for Pt-Fe and Pt-Mo catalysts in the hydrogenation of carbonyl groups. *Appl. Catal. B* **231**, 182–190 (2018).

18. Gao, X., Heyden, A., Abdelrahman, O. A. & Bond, J. Q. Microkinetic analysis of acetone hydrogenation over Pt/SiO_2. *J. Catal.* **374**, 183–198 (2019).

19. Basu, S. & Pradhan, N. C. Kinetics of acetone hydrogenation for synthesis of isopropyl alcohol over Cu-Al mixed oxide catalysts. *Catal. Today* **348**, 118–126 (2020).

20. Lu, S., Wu, J., Peng, H. & Chen, Y. Carbon-supported Raney nickel catalyst for acetone hydrogenation with high selectivity. *Molecules* **25**, 803 (2020).

21. Matanović, I. Selectivity control for electroreduction of ketones. *Nat. Catal.* **2**, 186–187 (2019).

22. Song, Y. et al. Hydrogenation of benzaldehyde via electrocatalysis and thermal catalysis on carbon-supported metals. *J. Catal.* **359**, 68–75 (2018).

23. Antonietta Casadei, M. & Pletcher, D. The influence of conditions on the electrocatalytic hydrogenation of organic molecules. *Electrochim. Acta* **33**, 117–120 (1988).

24. Li, Z. et al. Aqueous electrocatalytic hydrogenation of furfural using a sacrificial anode. *Electrochim. Acta* **64**, 87–93 (2012).

25. zhao, B., Chen, M., Guo, Q. & Fu, Y. Electrocatalytic hydrogenation of furfural to furfuryl alcohol using platinum supported on activated carbon fibers. *Electrochim. Acta* **135**, 139–146 (2014).

26. Zhang, X. et al. Simultaneously high-rate furfural hydrogenation and oxidation upgrading on nanostructured transition metal phosphides through electrocatalytic conversion at ambient conditions. *Appl. Catal. B* **244**, 899–908 (2019).

27. Zhang, W., Shi, Y., Yang, Y., Tan, J. & Gao, Q. Facet dependence of electrocatalytic furfural hydrogenation on palladium nanocrystals. *Chin. J. Catal.* **43**, 3116–3125 (2022).

28. Bondue, C. J., Calle-Vallejo, F., Figueiredo, M. C. & Koper, M. T. M. Structural principles to steer the selectivity of the electrocatalytic reduction of aliphatic ketones on platinum. *Nat. Catal.* **2**, 243–250 (2019).

29. Wu, Y., Guo, Z., Sun, C., Ren, X. & Li, Q. High-efficiency electrochemical hydrogenation of biomass-derived benzaldehyde compounds via a durable and versatile dendritic-like Pd/Cu-CF electrocatalyst. *Fuel Process. Technol.* **237**, 107436 (2022).

30. Anibal, J., Malkani, A. & Xu, B. Stability of the ketyl radical as a descriptor in the electrochemical coupling of benzaldehyde. *Catal. Sci. Technol.* **10**, 3181–3194 (2020).

31. Koh, K. et al. Electrochemically tunable proton-coupled electron transfer in Pd-catalyzed benzaldehyde hydrogenation. *Angew. Chem. Int. Ed.* **59**, 1501–1505 (2020).

32. Lopez-Ruiz, J. A. et al. Understanding the role of metal and molecular structure on the electrocatalytic hydrogenation of oxygenated organic compounds. *ACS Catal.* **9**, 9964–9972 (2019).

33. Luo, Y., Zhang, Z., Chhowalla, M. & Liu, B. Recent advances in design of electrocatalysts for high-current-density water splitting. *Adv. Mater.* **34**, 2108133 (2022).

34. Liu, K. et al. Intensified gas-phase hydrogenation of acetone to isopropanol catalyzed at metal-oxide interfacial sites. *Chem. Eng. J.* **454**, 140059 (2023).

35. Wang, X. et al. Insights into the shape effect of H_2 self-selective Ni catalysts for efficient acetone hydrogenation. *Appl. Surf. Sci.* **536**, 147844 (2021).

36. Tao, K., Li, W., Li, H. & Qi, X. Effect of modified industrial zeolite beta on one-step catalytic hydration of propene to isopropanol. *Appl. Catal. A Gen.* **139**, 43–49 (1996).

37. Ivanov, A. V., Zausa, E., Taârit, Y. B. & Essayem, N. Mechanism of propene hydration over heteropolyacid catalysts. *Appl. Catal. A Gen.* **256**, 225–242 (2003).

38. Shin, H., Hansen, K. U. & Jiao, F. Techno-economic assessment of low-temperature carbon dioxide electrolysis. *Nat. Sustain.* **4**, 911–919 (2021).

39. De Luna, P. et al. What would it take for renewably powered electrosynthesis to displace petrochemical processes? *Science* **364**, eaav3506 (2019).

40. Zhao, B.-H. et al. Economically viable electrocatalytic ethylene production with high yield and selectivity. *Nat. Sustain.* **6**, 827–837 (2023).

41. Massaro, M. C. & Monteverde, A. H. A. Techno-economic analysis of FDCA production through electrocatalytic processes. *J. Electrochem. Soc.* **169**, 054515 (2022).

Acknowledgements

Author contributions

J.Z. proposed and supervised the project. J.L. synthesized the catalysts. J.L., Z.L. and J.B. carried out the electrochemical experiments and related data processing. J.L., Z.W. and G.W. conducted materials characterization. H.W. and P.L. performed HRTEM characterization. Y.W. conducted the technoeconomic analysis. J.Z., Z.L. and J.L. cowrote the paper. P.L. and J.W. reviewed the paper. All authors discussed the results and commented on the paper.

Competing interests

J.Z. and J.L. are inventors on a patent application submitted by Northwestern Polytechnical University (CN116555785A), which covers the electrocatalytic hydrogenation of carbonyl compounds for the production of corresponding alcohols. The other authors declare no competing interests.

Additional information

Supplementary information The online version contains supplementary material available at https://doi.org/10.1038/s41929-025-01316-7.

Correspondence and requests for materials should be addressed to Pan Liu or Jian Zhang.